Fig. S1. Cell trajectory straightness by region. (**A**) Mean track straightness from four wild-type embryos. (**B**) Mean straightness from three *notum1a* over-expressing embryos. (**C**) Mean straightness from three SU5402-treated embryos. In wild-type embryos, the DM has the straightest tracks. The straightness decreases in the PZ ($P<0.05$) and further in the PSM ($P<0.05$). Upon ectopic *notum1a* expression, there is no significant decrease in mean track straightness. After SU5402 treatment, the track straightness is diminished in the DM ($P<0.05$) and PZ ($P<0.05$). *P*-values calculated by ANOVA.
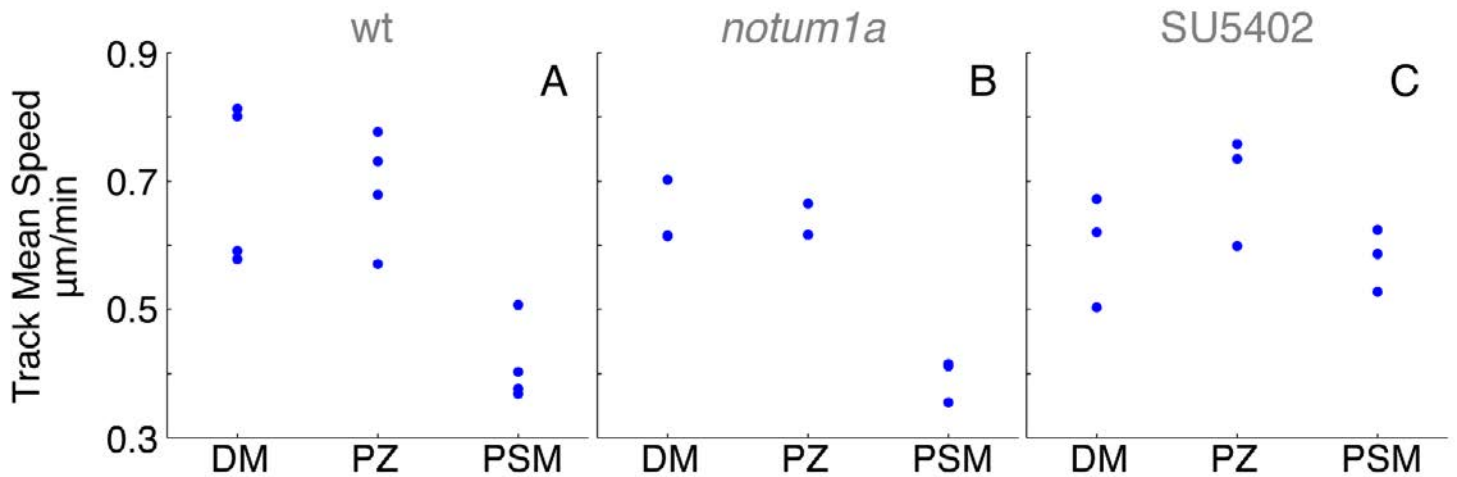

Fig. S2. Mean speeds of cell trajectories. (**A**) Means of four wild-type embryos. (**B**) Means of three *notum1a* over-expressing embryos. (**C**) Means of three SU5402-treated embryos. In wild-type embryos, the DM and PZ exhibit the highest track mean speeds. The mean speeds remains unchanged after ectopic *notum1a* expression. After SU5402 treatment, the mean speed of the PSM increases ($P<0.05$) becoming more similar to the DM and PZ. *P*-values calculated by ANOVA.
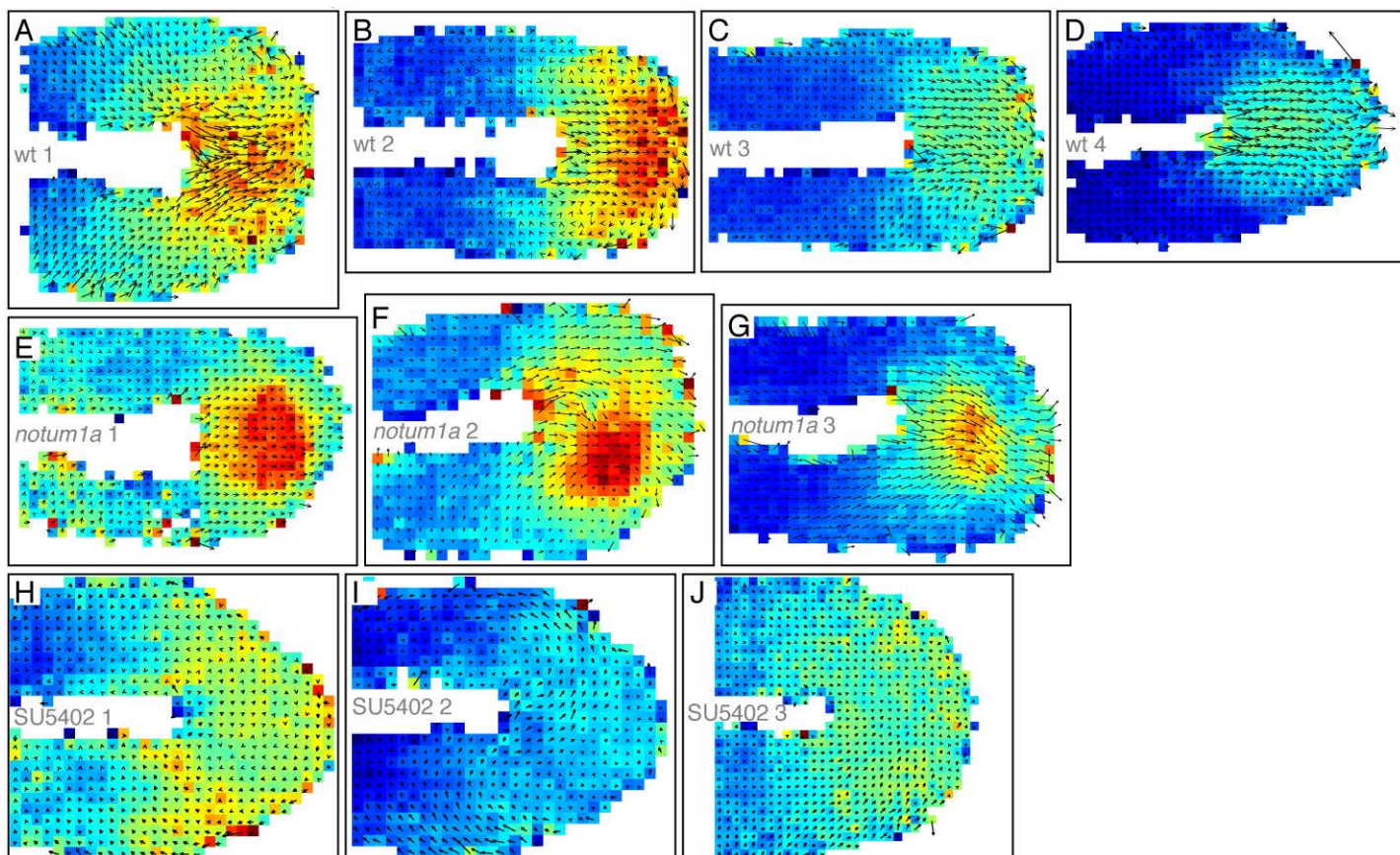
Fig. S3. Cell flow map of wild type, *notum1a* over-expressing embryos and SU5402-treated embryos. (A-J) The embryo was divided into sectors and an average 3D velocity vector was calculated for each sector (averaged in time and in the *z* dimension) using the individual cell velocities $\mathbf{v}_i$. The vector displacement map for the velocity was then obtained by plotting in each pixel the mean speed and the projection of the averaged 3D velocity vector. The heat map represents the average relative speed of the sector. The arrows are the 3D orientation of the averaged velocity vector. (A-D) Four wild-type embryos. (E-G) Three *notum1a* over-expressing embryos. (H-J) Three SU5402-treated embryos. Posterior is to the right.
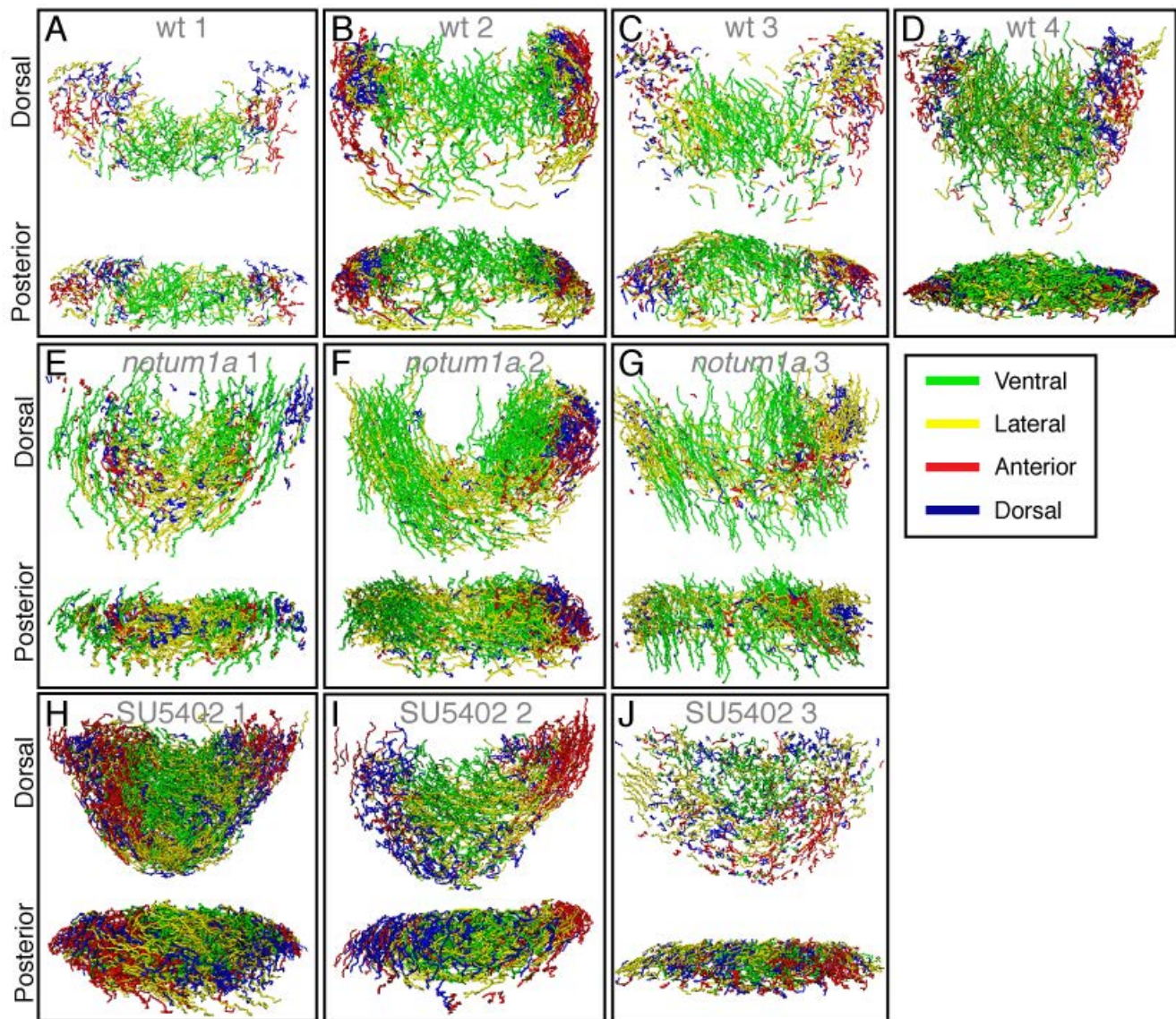
Fig. S4. Cell flow within the PZ as revealed by the cell trajectories in the top 10% displacement in each direction. (**A-D**) Four wild-type embryos. (**E-G**) Three *notum1a* over-expressing embryos. (**H-J**) Three SU5402-treated embryos. (A-D) In the wild-type PZ, the spatial segregation of the top 10% of tracks with the largest displacements reveal the bilateral flow of cells. Cells from the DM move ventrally into the medial PZ (green). Cells then flow laterally (yellow). Along the lateral edges where they are spatially segregated from the ventral flow, cells move anteriorly (red) and dorsally (blue). (E-G) In the *notum1a* over-expression embryos, the flow pattern loses its bilateral symmetry. (H-J) In the SU5402-treated embryos, the bilateral symmetry is better maintained than in *notum1a* embryos.
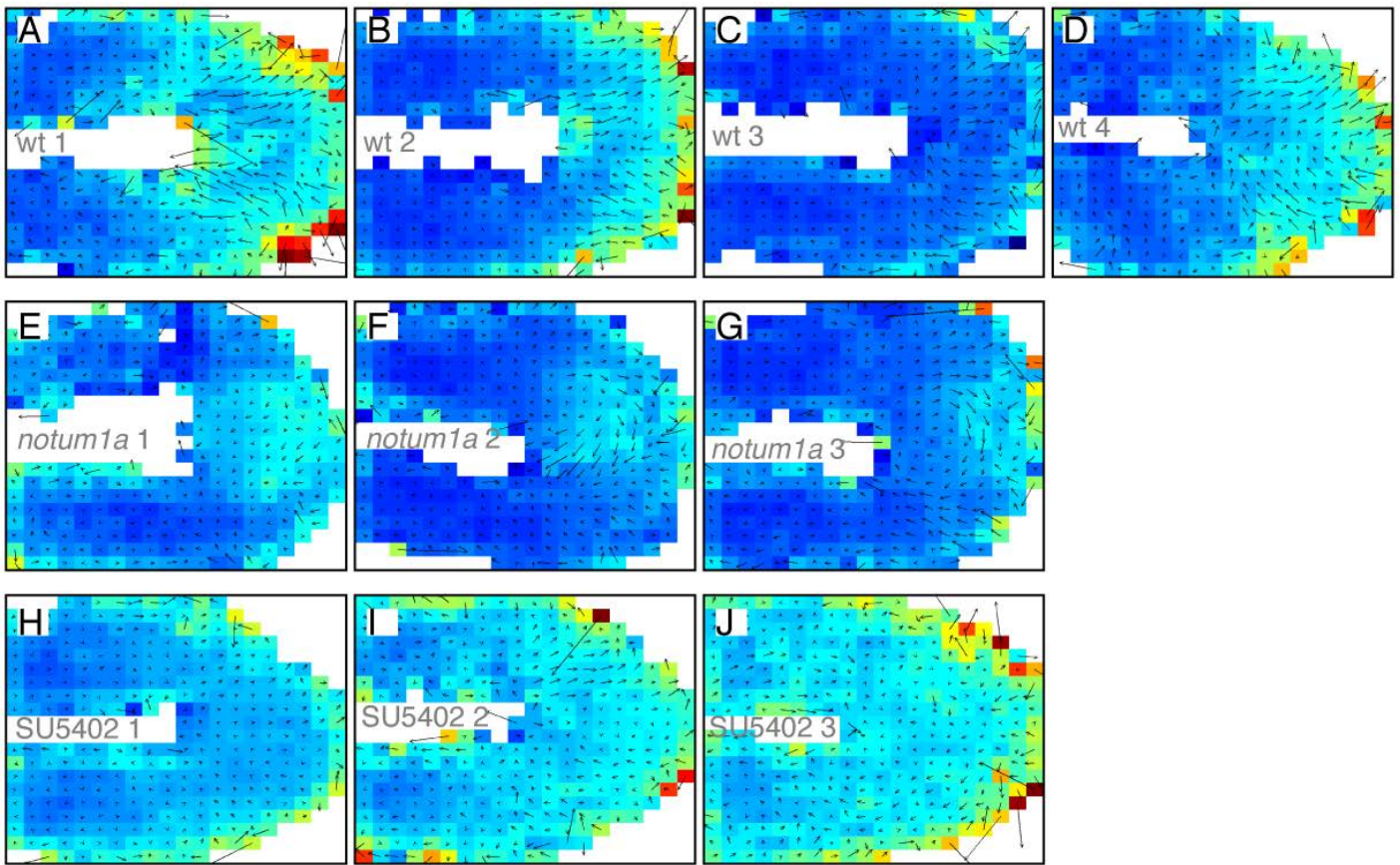
Fig. S5. Map of local rotational velocity within the cell flow field calculated via a 3D finite element mesh. Posterior is to the right. The heat map represents magnitude of the local rotational velocity. Arrows represent the direction of the rotation via the 'right-hand rule'. (**A-D**) Four wild-type embryos. (**E-G**) Three *notum1a* over-expression embryos. (**H-J**) Three SU5402-treated embryos. In the wild-type embryos, the local rotation reveals cells diving into the PZ from the DM (arrows slanting upwards). In the ectopic *notum1a* embryos, the diving is lost and the cells rotate up in the PZ (arrows slanting downwards). In the SU5402-treated embryos, the dorsal-to-ventral local rotation into the PZ from the DM is reduced but not reversed.
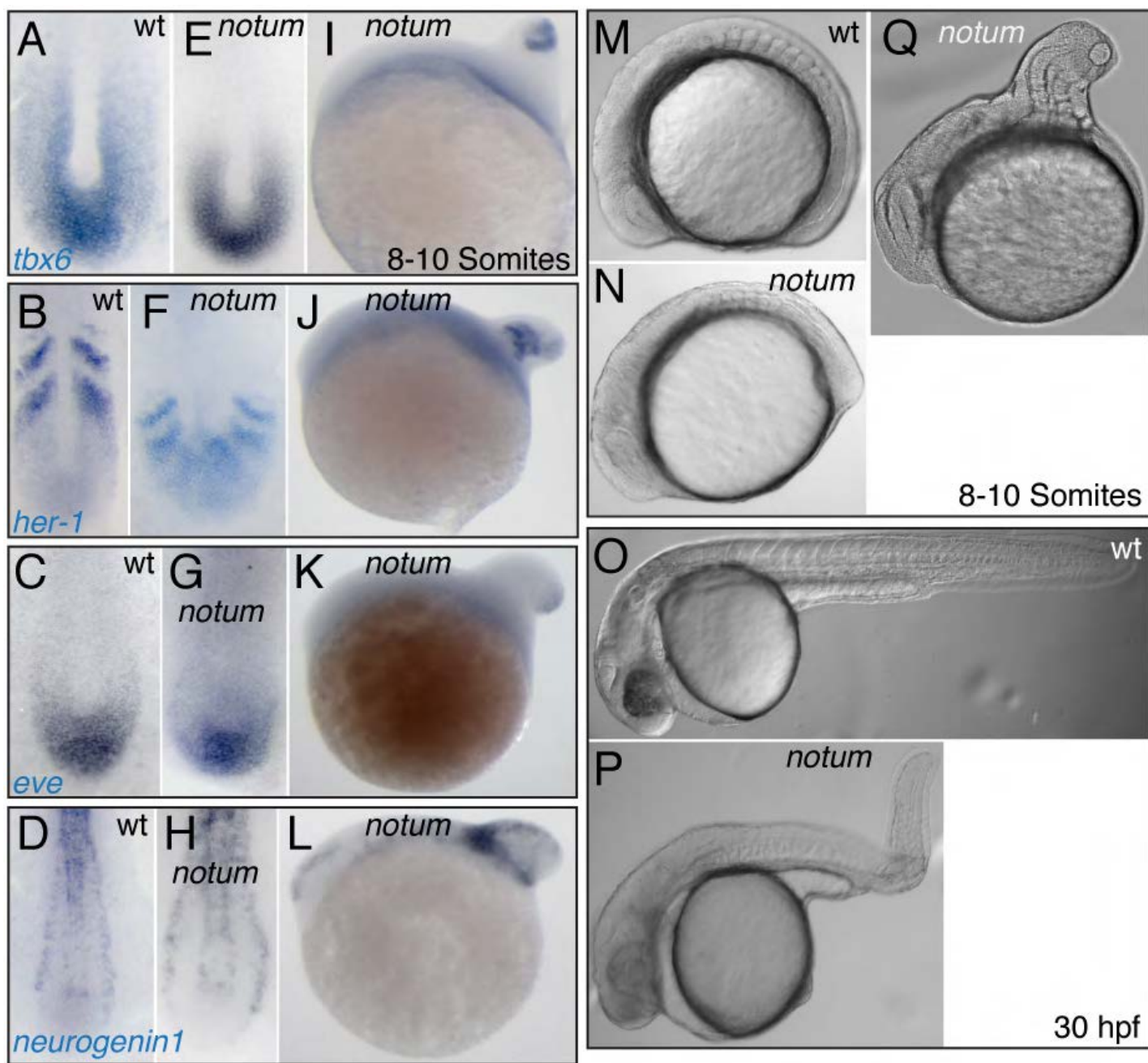
Fig. S6. *notum1a* over-expression phenotypes. (A-D,M,O) Wild type. (**E-H,N,P**) The moderate *notum1a* over-expression phenotype used for quantitative image analysis. (**I-L,Q**) The severe *notum1a* over-expression phenotype. The expression domains of mesodermal genes *tbx6* (A,E,I) *her1* (B,F,J) *eve* (C,G,K) and the neural gene *neurogenin1* (D,H,L) remain after ectopic *notum1a* expression indicating that *notum1a* retains patterned mesodermal and neural cell fates. (P) Roughly half of 'moderate phenotype class' embryos at 8-10 somites give rise to misdirected body axes at 30 hpf.
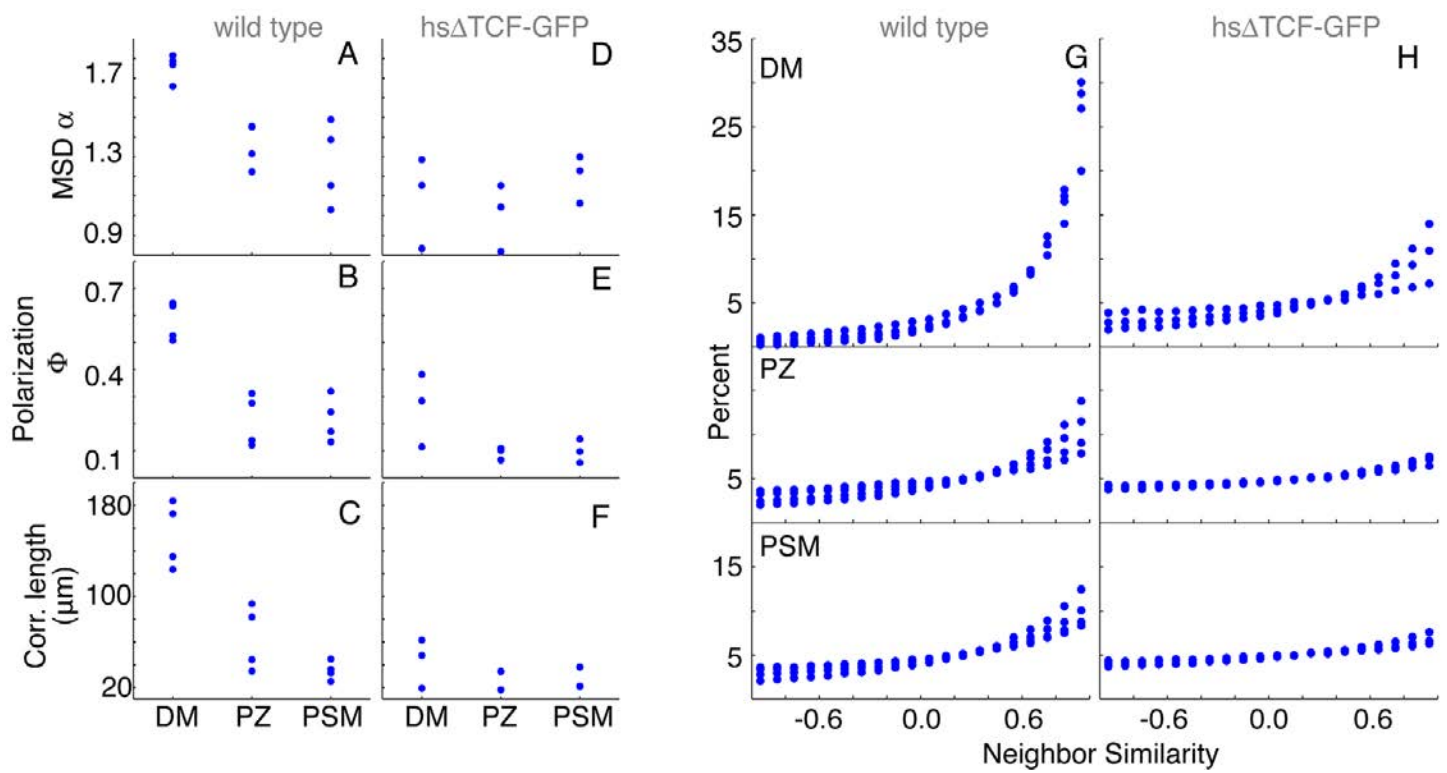
Fig. S7. Heat shock expression of hsΔTCF-GFP during trunk elongation causes a decrease in effective and coherent cell migration in the tailbud. (**A-C**,**G**) Data from the four wild-type embryos. (**D-F**,**H**) Data from three hsΔTCF-GFP embryos. These embryos have reduced effective migration (DM, $P<0.05$; PZ, $P<0.05$) (D), polarization (DM, $P<0.05$) (E), correlation length of the direction of motion (DM, $P<0.05$) (F) and neighbor similarity (H) compared with wild type. These alterations in cell flow are more severe than seen in *notum1a* over-expressing embryos. *P*-values calculated by Student's *t*-test.
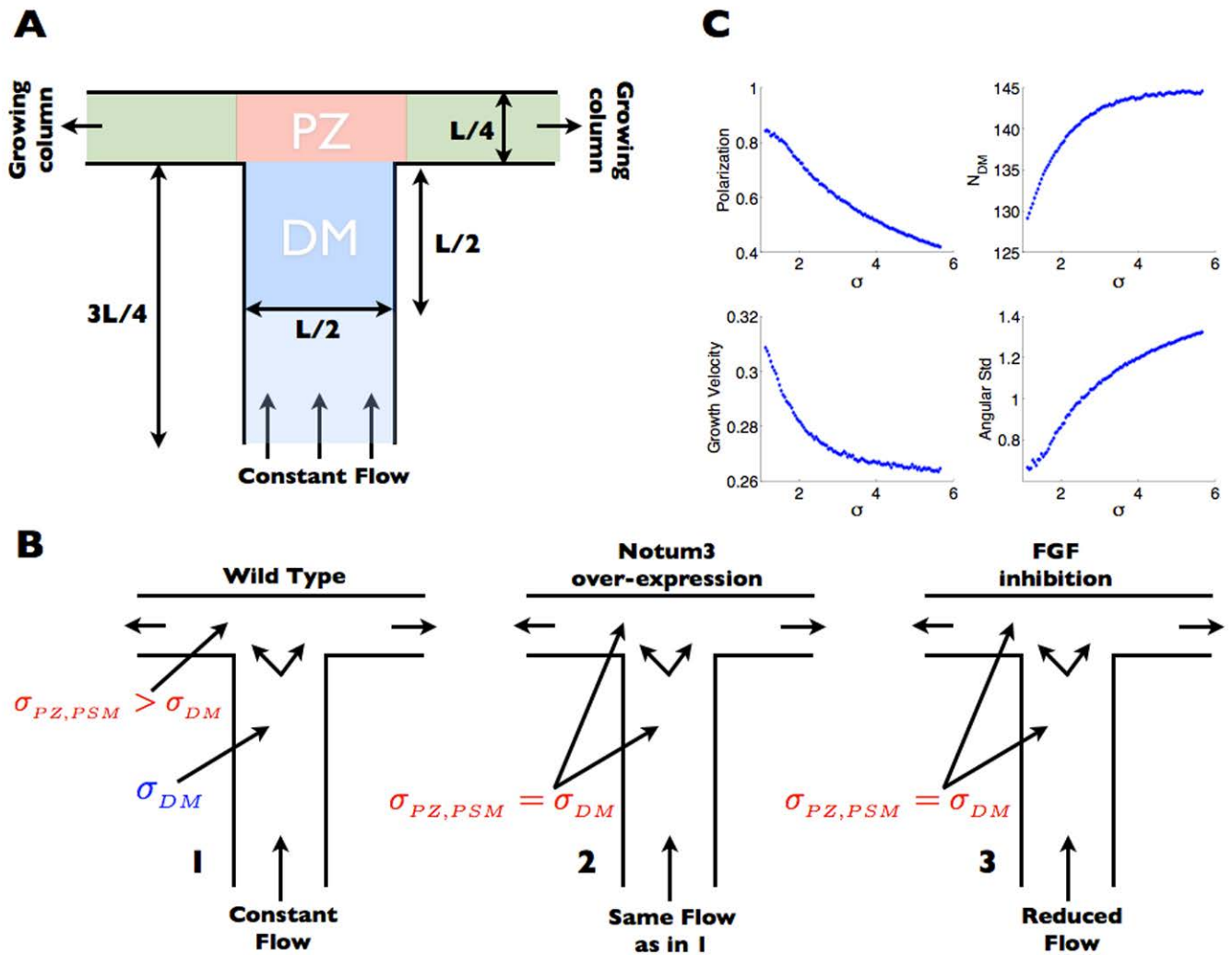
Fig. S8. A two-dimensional model of the tailbud cell flow. (**A**) The T-shape with dimensions labeled and the different regions showed in color. (**B**) The simulation set up for three different cases namely, (1) WT, (2) *notum3* over-expression and (3) FGF inhibition. (**C**) Variation of the Polarization, cell number in DM, rate of growth of the T-trunks, and the angular standard deviation as a function of noise strength in the DM. See Appendix S1 for additional details.

Andrew K. Lawton, Amitabha Nandi, Michael J. Stulberg, Nicolas Dray, Michael W. Sneddon, William Pontius, Thierry Emonet and Scott A. Holley. Regulated tissue fluidity steers zebrafish body elongation.

APPENDIX

Quantitative analysis of cell motion

Imaris software (Bitplane) was used to track the 3-D position of individual nuclei and extract basic statistics of motion. For an arbitrary cell i, with position vector $\mathbf{R}_i(t)$, the incremental displacement and the instantaneous velocity are given by $\Delta\mathbf{R}_i(t) = [\mathbf{R}_i(t + \Delta t) - \mathbf{R}_i(t)]$, and $\mathbf{v}_i(t) = \Delta\mathbf{R}_i(t)/\Delta t$ respectively, where Δt is the elapsed time. Before we started analyzing, the cell-position data for the entire tailbud was divided into different regions, namely the DM, PZ, and the PSM. This subdivision was done manually in Imaris by sorting tracks by physical location. For these different regions, we plotted the distributions of the instantaneous speeds, speed coefficient of variation (CV) and the track straightness. The CV of the speed is defined as the standard deviation of the cell-speeds divided by the mean speed, namely $\sqrt{\langle v_i^2(t)\rangle - \langle v_i(t)\rangle^2}/\langle v_i(t)\rangle$. The track straightness is simply the track displacement divided by the track length. Thus, a value of 1 represents a straight line. All the plots and further analysis of the cellular flow were performed in MatLab.

Establishing the reference frame

To correct for any drift or global movement of the tailbud, we quantified the cellular movement with respect to the anterior $50\ \mu m$ of the PSM which consistently displayed relatively minimal movement along the anterior-posterior axis. The center of mass velocity $\mathbf{v}_{CM}^{APSM}(t)$ was then calculated at each time point by averaging over all the cell

velocities in this region. The individual position and velocity of the cells in the tailbud were then corrected as,

$$\mathbf{r}_i(t) = \mathbf{R}_i(t) - \mathbf{v}_{CM}^{APSM}(t)\Delta t,$$
$$\mathbf{u}_i(t) = \mathbf{v}_i(t) - \mathbf{v}_{CM}^{APSM}(t). \tag{1}$$

We used $(\mathbf{r}_i, \mathbf{u}_i)$ to compute the Mean Square Displacement (MSD), Polarization, correlation functions, neighbor similarity, the polar and azimuthal angle of the instantaneous velocity and convergence and extension. These values were calculated for four wild-type embryos, three affected and three unaffected *notum1a* over-expressing embryos, three affected and three unaffected SU5402 treated embryos, three *cdh2* mutant embryos and three hsΔTCF-GFP embryos. The values were averaged for each group of embryos. The specifics of each metric are discussed in detail in the supplemental materials.

Mean Square Displacement (MSD)

The MSD for an individual cell track *i* is given by,

$$\left\langle \Delta \mathbf{r}_i^2(\tau) \right\rangle = \left\langle [\mathbf{r}_i(t+\tau) - \mathbf{r}_i(t)]^2 \right\rangle_T = \left\langle [x_i(t+\tau) - x_i(t)]^2 + [y_i(t+\tau) - y_i(t)]^2 + [z_i(t+\tau) - z_i(t)]^2 \right\rangle,$$

$$\tag{2}$$

where τ is the lag-time and the average is taken over the entire time trajectory *T*. The MSD function is then fitted by a power law

$$\left\langle \Delta \mathbf{r}_i^2(\tau) \right\rangle = A \times \tau^{\alpha}. \tag{3}$$

The exponent α carries information about the motion type: $\alpha = 1$ is Brownian and a ≈ 2 is ballistic. The prefactor A is proportional to the effective diffusion coefficient (in case of Brownian motion) or velocity (in the case of ballistic motion). We performed our MSD analysis on each individual track thus obtaining a distribution of A and α values by fitting Eq. (3). The α value was then averaged for the different regions of the embryo to obtain a mean α value.

Polarization

To quantify the degree of order in different regions of the embryo, we defined the Polarization (Cavagna, *et al*, 2010) as the average normalized velocity:

$$\Phi = \left\langle \left\| \frac{1}{N} \sum_{j=1}^{N} \frac{\mathbf{u}_j}{|\mathbf{u}_j|} \right\| \right\rangle_T . \tag{4}$$

Here the inner summation indicates average taken over the total number of cells (N) at each time and the outer bracket indicates the average over all times. For ordered behavior, Φ is close to 1 whereas for disordered behavior Φ is close to zero.

Spatial Correlation and Correlation Length Scale

A quantification of how the direction of cellular motion is correlated in space is achieved by calculating the two point correlation of the normalized velocities $\mathbf{n}_i = \mathbf{u}_i/|\mathbf{u}_i|$ (Bialek, *et al*, 2012):

$$C_\varphi(r) = \frac{\sum_{ij} (\mathbf{n}_i \cdot \mathbf{n}_j)\delta(r - r_{ij})}{\sum_{ij} \delta(r - r_{ij})}, \tag{5}$$

Here r_{ij} is the distance between the cell pairs and $\delta(r - r_{ij})$ is a smoothed Dirac delta function selecting cell pairs in $[r, r + dr]$. To estimate the characteristic distance over which the motion stays coordinated, we define a correlation length scale r_L which was obtained by fitting the initial decay of $C_\varphi(r)$ by an exponential function $C \exp(-r/r_L)$.

Neighbor Similarity

The neighbor similarity is a local measure of correlated movement and is written for any ij-th pair (Arboleda-Estudillo, *et al*, 2010) as:

$$S_{ij} = (\mathbf{n}_i \cdot \mathbf{n}_j)\left(1 - \Theta(r_{ij} - r_0)\right) = \cos\theta_{ij}\left(1 - \Theta(r_{ij} - r_0)\right). \tag{6}$$

Here θ_{ij} are the angles between the cell pairs and $\Theta(r_{ij} - r_0)$ is a Heaviside step-function. Only the neighboring pairs are considered, and we take the maximum distance between neighbors $r_0 \sim 20\,\mu m$ (assuming the average cell diameter is $\sim 10\,\mu m$). The neighbor similarity value can vary between -1 and +1 depending on whether the cells are moving in opposite or same direction.

Computing the polar angle of the instantaneous velocity

The polar angle ϕ is calculated using the following formula:

$$\phi = \tan^{-1}\left(\frac{u_y}{u_x}\right),$$

$$\tag{7}$$

where the x-axis is taken aligned along the anterior-posterior axis and the y-axis aligns with the medial-lateral axis. We calculated the standard deviation of the mean polar angle, namely $\sqrt{\langle\phi^2\rangle - \langle\phi\rangle^2}$, where the average was taken over all cells at all time-points.

Convergence and Extension

The rate of medial to lateral convergence and posterior extension for the ADM was calculated by measuring the change is size, both in the anterior-posterior and medial-lateral dimensions and dividing by the elapsed time. Size was measured by taking the difference of the terminal points at the first time point and at the last time point of the data set.

Smoothed Particle Hydrodynamics

The bulk behavior of the cellular movement in the posterior tailbud was studied by interpolating the velocity field between Lagrangian points (cell nuclei) and smoothing using Smoothed Particle Hydrodynamics (SPH): a mesh-free, particle based interpolation technique (Liu and Liu, 2010; Monaghan, 1992). In discrete time, the behavior of any physical quantity (velocity in our case) at an arbitrary point in space (inside the domain of interest) is obtained by taking a weighted average over a local neighborhood. For a detailed discussion on SPH, refer to (Liu and Liu, 2010; Monaghan, 1992).

The interpolation of any physical quantity $f_S(\mathbf{r})$ using SPH at a given instant of time can be written as,

$$f_S(\mathbf{r}) = \sum_{j=1}^{N} f_j \Omega_j W(\mathbf{r} - \mathbf{r}_j, h). \qquad (8)$$

Here r is an arbitrary point inside the volume. W is a smoothing kernel and h is the spatial width over which the smoothing is performed. The sum is taken over all the cell positions measured at each time. Each cell j at a position $\mathbf{r}_j$ has a volume Ω_j and the value of the physical quantity is f_j.

In our study we want to estimate the bulk movement of the cells, as well as the behavior when the bulk field is removed from the individual cell velocities. We therefore interpolate the velocities exactly at the cell positions. Defining $\Omega = m/\rho$, where m is the mass and ρ is the density, the bulk velocity $\mathbf{v}_i^B$ at position i is given by,

$$\mathbf{v}_i^B = \sum_{j=1}^{N} \mathbf{v}_j \frac{m_j}{\rho_j} W(\mathbf{r}_i - \mathbf{r}_j, h). \qquad (9)$$

Assuming the mass of the individual cells to be constant ($m_j \approx m$), the density at each cell location can then be calculated as,

$$\rho_i = \sum_{j=1}^{N} \rho_j \frac{m_j}{\rho_j} W(\mathbf{r}_i - \mathbf{r}_j, h) = m \sum_{j=1}^{N} W(\mathbf{r}_i - \mathbf{r}_j, h), \qquad (10)$$

which is then used in Eq. 9.

The smoothing kernel must be a normalized function, satisfying the following property,

$$\lim_{h \to 0} W(\mathbf{r} - \mathbf{r}', h) = \delta(\mathbf{r} - \mathbf{r}'), \qquad (11)$$

where $\delta(\mathbf{r} - \mathbf{r}')$ is the Dirac delta function. Eq. 11 ensures that with decreasing h, the smoothened function value approaches the actual function value. A proper kernel should also be compactly supported, namely $W(\mathbf{r} - \mathbf{r}', h) = 0, |\mathbf{r} - \mathbf{r}'| > \alpha h$ (α is a scaling factor). This ensures that the smoothing is performed strictly inside the local window defined by h (Liu and Liu, 2010). A low degree polynomial (cubic or a quartic spline) is a common choice for smoothing kernels that have good compact support and are computationally fast (Liu and Liu, 2010). Here we choose a quartic smoothing function (Liu, *et al*, 2003),

$$W(R,h) = C_d \begin{cases} \left(\dfrac{2}{3} - \dfrac{9}{8}R^2 + \dfrac{19}{24}R^3 - \dfrac{5}{32}R^4 \right), & 0 \le R \le 2, \\ 0, & R > 2, \end{cases} \qquad (12)$$

where $R = |\mathbf{r} - \mathbf{r}'|/h$. Here C_d is the normalization constant (d is the dimension), for $d = 3$, $C_d = 315/208\pi h^3$. Before using this kernel for our data, we tested it to estimate known functions. For the analysis of zebrafish tailbud data, we varied $h = 5\,\mu m$ to $40\,\mu m$ in steps of $5\,\mu m$.

One complication of using SPH for smoothing is implementing proper boundary conditions for complex shapes. One way to minimize the effect of boundaries is by choosing a small smoothing radius. On the other hand since we want to extract the bulk cellular movement in the embryo, too small value of the smoothing radius h will fail to do so. Here we show the data for radius ($h = 15\,\mu m$) that can smooth over a larger spatial extent, without introducing significant boundary effects.

We studied the fluctuations of the cell movement in the tailbud after removing the bulk motion, namely,

$$\Delta \mathbf{v}_i = \mathbf{v}_i - \mathbf{v}_i^B. \qquad (13)$$

Finite element method

Finite element method (FEM) is a computer aided mathematical technique (Burnett, 1987), which is often used to obtain approximate numerical solutions of partial differential equations, describing a physical system. Here we used FEM following established procedures from the field of fluid mechanics to extract velocity fields from

the Lagrangian velocities of the individual nuclei. (Kelley and Ouellette, 2011; Lee and Schachter, 1980). This allows us to look at the spatial variations of the velocity fields and quantify local rates of rotation and divergence.

For each time snap-shot, a tetrahedral mesh was constructed from the cell data using Delaunay triangulation (Lee and Schachter, 1980) such that no point lay in the circumcircle of any triangle. Once the mesh was created we defined a velocity function for each tetrahedron. If $T = \{a, b, c, d\}$ are the four vertices of a tetrahedron with coordinates $[(a_x, a_y, a_z), (b_x, b_y, b_z), (c_x, c_y, c_z), (d_x, d_y, d_z)]$, then the velocity function on this tetrahedron can be written in terms of the linear basis functions as,

$$v(x,y,z) = v(a)\phi_a(x,y,z) + v(b)\phi_b(x,y,z) + v(c)\phi_c(x,y,z) + v(d)\phi_d(x,y,z),$$

(14)

where $\phi's$ are the linear basis functions. Given Eq. (14), we can evaluate $v(x, y, z)$ (or its derivative) anywhere in the tetrahedron provided we know the correct basis functions. The basis functions $\phi's$ are chosen such that there is one basis function per vertex and the basis function of the ith vertex satisfies $\phi_i(j) = \delta_{i,j}$, where $\delta_{i,j}$ is the Kronecker delta function. In the present example, they are written as (Burnett, 1987),

$$\phi_a(x,y,z) = \frac{1}{6V} \begin{vmatrix} 1 & 1 & 1 & 1 \\ x & b_x & c_x & d_x \\ y & b_y & c_y & d_y \\ z & b_z & c_z & d_z \end{vmatrix}, \phi_b(x,y,z) = \frac{1}{6V} \begin{vmatrix} 1 & 1 & 1 & 1 \\ a_x & x & c_x & d_x \\ a_y & y & c_y & d_y \\ a_z & z & c_z & d_z \end{vmatrix},$$

$$\phi_c(x,y,z) = \frac{1}{6V} \begin{vmatrix} 1 & 1 & 1 & 1 \\ a_x & b_x & x & d_x \\ a_y & b_y & y & d_y \\ a_z & b_z & z & d_z \end{vmatrix}, \phi_d(x,y,z) = \frac{1}{6V} \begin{vmatrix} 1 & 1 & 1 & 1 \\ a_x & b_x & c_x & x \\ a_y & b_y & c_y & y \\ a_z & b_z & c_z & z \end{vmatrix},$$

(15)

where the vertical bars denote the determinant operation and V is the volume of the tetrahedron given by,

$$V = \frac{1}{6} \begin{vmatrix} 1 & 1 & 1 & 1 \\ a_x & b_x & c_x & d_x \\ a_y & b_y & c_y & d_y \\ a_z & b_z & c_z & d_z \end{vmatrix}.$$

(16)

Using $v(x,y,z)$ we calculated the vorticity in the velocity fields which is simply,

$$\vec{\Lambda} = \vec{\nabla} \times \vec{v}(x,y,z) = \begin{vmatrix} \hat{x} & \hat{y} & \hat{z} \\ \frac{\partial}{\partial x} & \frac{\partial}{\partial y} & \frac{\partial}{\partial z} \\ v_x & v_y & v_z \end{vmatrix}.$$

(17)

We divided the whole embryo into voxels and an average local rotational velocity was assigned to each sector. A two dimensional projection of the embryo was then obtained by averaging over all the sectors in the third dimension (the averaging is done for both the vectors and their absolute values). This was then plotted similar to the vector displacement map for the velocities.

Computer Model and Simulations

We consider a two-dimensional model of self-propelled motion with polar alignment based on the study by Szabó et. al., (Szabo, *et al*, 2006). Each cell is modeled as a soft particle of radii a_i with an instantaneous position r_i (the center of the particle). The overdamped dynamics of the *i*th cell is given by,

$$\dot{\mathbf{r}}_i = v_0 \hat{\mathbf{n}}_i + \mu \sum_{j=1}^{N} \mathbf{F}(\mathbf{r}_i, \mathbf{r}_j)$$

$$\dot{\theta}_i = \frac{1}{\tau} \sin^{-1}\left[\left(\hat{\mathbf{n}}_i \times \hat{\mathbf{r}} \right) \cdot \hat{\mathbf{z}} \right] + \xi_i.$$

$$(18)$$

The cells move with a self-propelling velocity $v_0 \hat{\mathbf{n}}_i$ of constant speed v_0 and mobility μ and experience forces by the neighboring cells via $\mathbf{F}(\mathbf{r}_i, \mathbf{r}_j)$. The unit vector $\hat{\mathbf{n}}_i = (\cos\theta_i, \sin\theta_i)$ defines the cellular polar direction, i.e. the direction of the self-propelling velocity. This polar axis tends to align along the direction of cellular velocity $\hat{\mathbf{r}} = \dot{\mathbf{r}}_i / |\dot{\mathbf{r}}_i| = (\cos\varphi_i, \sin\varphi_i)$ with a relaxation time τ and an angular noise denoted by ξ_i. The quantity ξ_i is a delta-correlated white noise with zero mean.

The interaction between cells is short ranged and modeled by a piecewise linear force-function which is given by,

$$\mathbf{F}(\mathbf{r}_i, \mathbf{r}_j) = \hat{\mathbf{r}}_{ij} \begin{cases} F_{rep} \dfrac{(R_{eq} - r_{ij})}{R_{eq}}, & r_{ij} < R_{eq}, \\[2mm] F_{adh} \dfrac{(R_{eq} - r_{ij})}{\alpha R_{eq}}, & R_{eq} \le r_{ij} \le (1+\alpha)R_{eq}, \\[2mm] 0, & r_{ij} > (1+\alpha)R_{eq}. \end{cases} \qquad (19)$$

Here $r_{ij} = |\mathbf{r}_i - \mathbf{r}_j|$, and $\hat{\mathbf{r}}_{ij}$ is the corresponding unit vector. F_{rep} and F_{adh} are the maximum repulsive and adhesive force values. The equilibrium distance between two cells is given by $R_{eq} = (a_i + a_j)$. The parameter α sets the upper bound for the short ranged attraction and is taken to be a small quantity (< 1). For details of the model please refer to (Szabo, *et al*, 2006; Vicsek and Zafeiris, 2012).

Parameter Values

To study Eq. (18) numerically we use particles whose radii are uniformly distributed in $a \in [a_0 - \delta, a_0 + \delta]$, where $2a_0 = 5/6$ is the average cell diameter and we choose $\delta = 0.05$. We set $v_0 = 1, \mu = 1, \tau = 1, F_{rep} = 32, F_{adh} = 0.95, \alpha = 0.2$ for the simulations. The magnitude of the angular noise is chosen from a uniform distribution in the interval $\frac{\sigma}{\sqrt{\Delta t}}\left[-\frac{\pi}{2}, \frac{\pi}{2}\right]$, where σ is the control parameter. The time-step of integration is taken to be $\Delta t = 0.005$. For our simulations we set the initial number density to a high value (close to unity) to ensure the onset of collective motion and also to mimic the conditions in a real tissue where the cells are closely packed. As a result the absolute noise strength required to represent the WT situation (such that the angular distribution agrees with those obtained from experiments) is also high.

Simulations

We perform the simulations on a geometric structure that resembles a 'T' in 2D with reflective walls (A). This is an oversimplification of the actual 3D geometry of the tailbud representing the collective behavior across the DM into the PZ, followed by a bilateral division. In our model the lower column of the T represents the DM region and the upper part is representative of the PZ region (A). Particles are introduced at a constant rate

from below. They move forward and divide bilaterally in the PZ, and then move out along the two trunks of the T. Unlike the real embryo, where the tip of the tailbud grows in the forward direction, the upper wall of the T here is held fixed. Similarly the two trunks of the T can be considered to be representative of the two PSMs: however in contrary to the real PSMs which grows towards the posterior direction, they are allowed to grow freely outside and as a result the velocity of the particles do not go to zero (as it does in the PSM). Here, we aim to understand the changes in the collective behavior as a function of cellular polar direction and cellular flow in the DM region only. A simpler geometric shape like a rectangular column (where particles flow in at a constant rate from one side and are allowed to grow on the other side) would be sufficient to illustrate the interplay between influx, coherence of the cellular flow and jamming. However, we utilize the T-shape due to a closer resemblance to the tailbud geometry.

To compare the different scenarios of collective motion as seen in the experiments, we vary only two parameters, namely the angular noise amplitude σ and the cellular flow-rate at the inlet (bottom of the T). The dimension of the T-shape is shown in (A). L is chosen in such a way that $N_0 = L / 4a_0 \sim 10$.

We simulate the WT situation (Panel B, case 1) by pushing particles with angular noise $\sigma_{DM} = 1.4$ into the T at a constant rate ($(N_0 - 2)$ particles in every $N_{steps} = \gamma / (v_0 \Delta t)$ iteration steps). Here γ is a parameter to control the flow, which is set to $\gamma = 1.5$. The angular noise in the PZ is kept higher ($\sigma_{PZ,PSM} = 5.6$). As a result the polarization and correlation length of the simulated cells motion are smaller in the PZ than in the DM mimicking experimental data.

In the experiments, over-expression of *notum*3 leads to reduced polarization and flow rate in the DM but not in the ADM. (Panel B, case 2). We simulated this using the stronger angular noise ($\sigma = 5.6$) everywhere but keeping the influx of cells at the bottom of the T the same as for the WT case ($\gamma = 1.5$).

Finally, we simulate the FGF inhibition case (panel B, case 3) using the same high angular noise everywhere as for *notum3* overexpression along with a reduced flow ($\gamma = 3$). The cellular motion in the DM region is quantified by calculating the Polarization (Φ), the angular standard deviation, and mean number of cells. Note that these measures are calculated on a small time-window after removal of initial transients (the same amount of transient for all the different cases), and then averaged over 100 different stochastic runs. Since the number density is time-dependent, for the case of high angular noise, taking a longer time window introduces artifacts due to inability of the walls to adjust to increasing cell number in this simple model.

We also studied the variation of the various measures, as a function of noise intensity (panel C) in the DM (σ is set constant at 5.6 in the top column, and varied in DM). With increasing angular noise the Polarization goes down, whereas the Number of cells in the DM and the angular standard deviation goes down. We quantified an additional measure, namely the growth velocity of the T trunks, which goes down with increasing noise.

References

Arboleda-Estudillo, Y., Krieg, M., Stuhmer, J., Licata, N. A., Muller, D. J. and Heisenberg, C. P. (2010) Movement directionality in collective migration of germ layer progenitors. *Curr Biol*, **20**, 161-169.

Bialek, W., Cavagna, A., Giardina, I., Mora, T., Silverstri, E., Viale, M. and Walczak, A. M. (2012) Statistical mechanics of natural flocks of birds. *Arxiv:1107.0604v1*.

Burnett, D. S. (1987) *Finite Element Analysis: From Concepts to Applications*. Reading, MA: Addison-Wesley Publishing Co.

Cavagna, A., Cimarelli, A., Giardina, I., Parisi, G., Santagati, R., Stefanini, F. and Viale, M. (2010) Scale-free correlations in starling flocks. *Proc Natl Acad Sci U S A*, **107**, 11865-11870.

Kelley, D. H. and Ouellette, N. T. (2011) Onset of three-dimensionality in elecromagnetically driven thin-layer flows. *Phys. Fluids*, **23**, 045103.

Lee, D. T. and Schachter, B. J. (1980) Two Algorithms for Constructing a Delaunay Triangulation. *Int J Computer Information Sci*, **9**, 219-242.

Liu, M. B. and Liu, G. R. (2010) Smoothed Particle Hydrodynamics (SPH): an Overview and Recent Developments. *Arch Comput Method E*, **17**, 25-76.

Liu, M. B., Liu, G. R. and Lam, K. Y. (2003) Constructing smoothing functions in smoothed particle hydrodynamics with applications. *J Comput Appl Math*, **155**, 263-284.

Monaghan, J. J. (1992) Smoothed Particle Hydrodynamics. *Annu Rev Astron Astr*, **30**, 543-574.

Szabo, B., Szollosi, G. J., Gonci, B., Juranyi, Z., Selmeczi, D. and Vicsek, T. (2006) Phase transition in the collective migration of tissue cells: experiment and model. *Physical review. E, Statistical, nonlinear, and soft matter physics*, **74**, 061908.

Vicsek, T. and Zafeiris, A. (2012) Collective motion. *Physics Reports*, **in press**, 1-70.